Characterization of grain structure in nanocrystalline gadolinium by high-resolution transmission electron microscopy

Martin Seyring[a)]
Institute of Materials Science and Technology, Friedrich Schiller University, D-07747 Jena, Germany

Xiaoyan Song
College of Materials Science and Engineering, Beijing University of Technology, Beijing 100022, People's Republic of China

Andrey Chuvilin and Ute Kaiser
Electron Microscopy Group of Materials Science, University of Ulm, D-89081 Ulm, Germany

Markus Rettenmayr
Institute of Materials Science and Technology, Friedrich Schiller University, D-07747 Jena, Germany

(Received 15 April 2008; accepted 8 August 2008)

A method is presented for recognition of nanograins in high-resolution transmission electron microscope (HRTEM) images of nanocrystalline materials. We suggest a numerical procedure, which is similar to the experimental dynamic hollow cone dark-field method in transmission electron microscopy and the annular dark-field method in scanning transmission electron microscopy. The numerical routine is based on moving a small mask along a circular path in the Fourier spectrum of a HRTEM image and performing at each angular step an inverse Fourier transform. The procedure extracts the amplitude from the Fourier reconstructions and generates a sum picture that is a real space map of the local amplitude. From this map, it is possible to determine both the size and shape of the nanograins that satisfy the selected Bragg conditions. The possibilities of the method are demonstrated by determining the grain size distribution in gadolinium with ultrafine nanocrystalline grains generated by spark plasma sintering.

I. INTRODUCTION

Nanocrystalline structures exhibit properties that are different from conventional coarse-grained structures. The unique properties result from both the reduced grain size and the large fraction of grain boundaries. Grain size and the grain size distribution (GSD) are important parameters for characterizing the structure of the nanoscale materials. To evaluate the detailed relation between properties and structure of nanocrystalline materials, it is necessary to determine the GSD. Nanocrystalline bulk metals prepared by spark plasma sintering of nanoscaled powders of rare earth metals[1,2] show a significant change in mechanical and physical properties, as compared with the polycrystalline rare earth metals. However, the GSD features in the nanocrystalline metal bulks have rarely been characterized in literature,[3–5] which should be necessary to correlate the microstructure characteristics with the properties of the nanomaterials.

In general, there are several techniques in transmission electron microscopy (TEM) and x-ray diffraction (XRD) to determine the GSD in nanocrystalline materials, each with its own advantages and drawbacks. Estimation of the GSD from an XRD-pattern is sensitive to the applied analysis method.[6] Assumptions have to be made about the shape of the grains and the specific shape of the function of the GSD.[7] Therefore an approximated GSD needs to be compared with TEM results. Without knowledge about the shape of the distribution function, it is not possible to measure the GSD in nanocrystalline Gd via XRD.

TEM offers high-resolution TEM (HRTEM)[8] and also several dark-field techniques to measure the nanograin size directly, such as centered dark field (CDF),[6] annular dark field (ADF), or high angle annular dark field (HAADF) in scanning transmission microscopy (STEM).[9] HRTEM was chosen to study the nanocrystalline grain structure and measure the GSD.

HRTEM images show directly the translational symmetry of the crystal lattice in a material. The nanograins are identified and discriminated by the emergence of lattice fringes[10] [Fig. 1(a)]. The appearance of too many features in the image (e.g., generation of moiré pattern by overlap of grains[11]) make it difficult to determine the contours of the nanograins from a simple evaluation of the image.

Hÿtch and Gandais developed a technique to extract nanograins by Fourier filtering of HRTEM images.[10] The method decomposes the HRTEM lattice image in

[a)]Address all correspondence to this author.
e-mail: martin.seyring@uni-jena.de
DOI: 10.1557/JMR.2009.0071

 © 2009 Materials Research Society

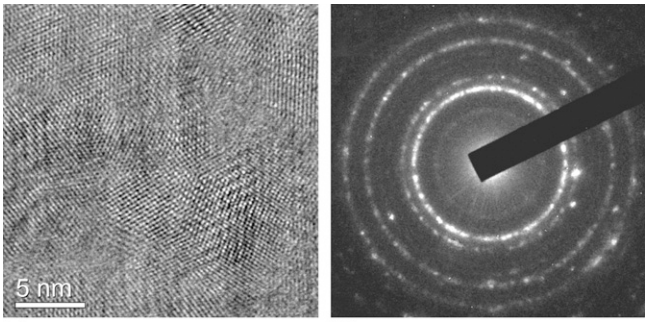

FIG. 1. HRTEM micrograph of (a) nanocrystalline Gd and (b) corresponding SADP.

a map of the amplitude and a map of the geometrical phase. This procedure has been applied a few times to analyze complex structures on the nanoscale from HRTEM images quantitatively: the method based on the analysis of the amplitude is successfully adapted to measure the three-dimensional (3D) morphology of colloidal CdS nanocrystals,[12] highlight nanocrystals in an amorphous matrix[10] and in powders,[13] and observe size and morphology of the particles.[14] To the best of our knowledge, the method has never been applied to measure the GSD in compact nanocrystalline materials. For this purpose, the method of Hÿtch and Gandais needs to be adapted. In the present article, the method of Hÿtch and Gandais was extended to generate an amplitude map that contrasts different orientated nanograins and excludes less pronounced nanograins. Since the contrasted areas correspond to the two-dimensional projected areas of the nanograins, the procedure is applied to calculate the GSD of nanocrystalline Gd.

II. EXPERIMENTAL

A. Sample preparation

The nanocrystalline Gd was produced by a combination of inert gas condensation and spark plasma sintering in an entirely closed system. A more detailed description of the synthesis of nanocrystalline pure rare-earth metals can be found elsewhere.[1,2] From the available Gd samples, two TEM foils were prepared using mechanical grinding and low-angle Ar-ion milling. Dimple grinding was avoided to keep the oxidation of the material on a low level.

B. Electron microscopy

The HRTEM observation was carried out on a JEM 3010 TEM/STEM (HR pole piece, JEOL, Tokyo, Japan) equipped with a multi scan 1k × 1k Gatan charge coupled device (CCD) camera (Pleasanton, CA). Studies were performed at 300 kV. Due to random grain orientation, some of the nanograins appear close to Bragg conditions and thus produce lattice fringes.

The HRTEM micrographs were taken at a magnification of 400,000. This magnification was found to be optimum, providing reasonable field of view and at the same time reasonable sampling of the lattice fringes on the CCD (approximately half Nyquist frequency). It is a compromise between different favorable conditions. To be as selective as possible, each Bragg spot of the Fourier spectrum should be far away from the origin, which is the case at low magnifications. On the other hand, a high magnification offers a better opportunity to analyze the nanograins. The image processing of the pictures was performed in the Digital Micrograph (Gatan) framework using homemade scripts.

III. IMAGE PROCESSING

In a HRTEM image, the nanograins are represented as a self-contained area consisting of one or more sets of lattice fringes. The lattice fringes are sinusoidal waves of intensity with a specific amplitude A_g and a specific geometrical phase P_g.[10] Their wavelength depends on the reciprocal lattice vector g of the corresponding lattice planes. Thus, the intensity I as a function of the position r in an HRTEM image of the crystalline structure can be written as a Fourier sum [Eq. (1)]:

$$I(r) = \sum_g A_g(r)\exp\left[iP_g(r)\right]\exp(i2\pi gr) \quad . \qquad (1)$$

Fourier filtering is an image processing technique often used in HRTEM to improve image contrast by placing a mask around Bragg spots in the Fourier spectrum. Via Fourier filtering, it is possible to decompose the image in terms of amplitude $A_g(r)$ and geometrical phase $P_g(r)$. The theoretical basis of this method was first described by Hÿtch and Gandais in Ref. 10, explained extensively in Refs. 15 and 16, and further developed in Ref. 17. To image the nanograins, the amplitude is isolated as a function of position $A_g(r)$. The amplitude is the envelope function of sinusoidal lattice fringes and displays the local degree of contrast of a set of fringes.[15] A two-dimensional fast Fourier transform (FFT) was applied to the HRTEM images [Figs. 2(a) and 2(b)]. The resulting FFT signal spectra display the distribution of the spatial image frequencies in the reciprocal space. Each Bragg spot in the FFT spectrum represents a set of lattice fringes with a specific distance $1/g$ and a specific orientation. The arrangement of several Bragg spots on concentric rings in the FFT spectra indicates the existence of several grains with different orientation in the original image. The radius of each ring corresponds to a particular interplanar spacing $1/g$.

At these rings, a circular path of 180° was defined to record all possible orientations of lattice fringes [black arrow in Fig. 2(b)]. During the numerical routine, a square window moves along the path with a step width

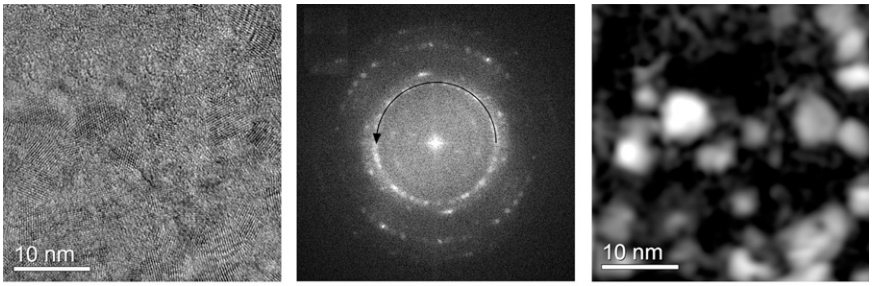

FIG. 2. HRTEM micrograph of (a) nanaocystalline area, (b) corresponding FFT with one of three possible paths of Gaussian filter, and (c) amplitude map displaying grains generated along path in (b).

of 5°. The step width was adapted on the one hand to yield sufficient resolution for distinguishing twins from each other and on the other hand to avoid selecting some grains twice. At each step, a spot of the FFT spectrum is chosen as the reciprocal lattice vector g; the value of g is calculated by the center of mass in the square window. Then a mask is applied to the position of g in the reciprocal space. The amplitude image is generated from the back-transformed image by calculating its modulus.

After the whole cycle, all the single maps of amplitude are added up to one sum picture [Fig. 2(c)]. For every chosen interplanar spacing, a sum picture is generated that shows the local contrast of the corresponding lattice fringes.

The quality of the amplitude map strongly depends on the size and shape of the mask $M(k)$ applied in reciprocal space.[15] A circular Gaussian hat was chosen as a mask to reduce the noise and to smooth the amplitude maps. Its diameter was adapted on the one hand to reduce the lateral resolution only as little as possible and on the other hand to enhance the averaging in real space to minimize the background noise. The compromise leads to some residual noise in the filtered image. To improve the signal-to-noise ratio, only the strongest Fourier components are selected. These correspond to the smallest rings in the Fourier spectrum. Only if the brightest pixel in the square window has an intensity larger than 1/4000 of the maximum intensity in the Fourier spectrum is an inverse FFT applied. Selecting spots with a lower intensity than 1/4000 results in amplitude single maps with a signal to noise ratio lower than 2. To enhance the resulting contrast, the intensity of each single map is squared.

Since the Fourier spectra of HRTEM images are related to the diffraction pattern, the generated amplitude images are related to dark-field images.[18] Therefore, the method can be referred to as numerical dynamic hollow cone dark field.

The gray levels in the amplitude images depend on the amplitude of the related lattice fringes. White represents a high and black a low amplitude. Usually different grains are represented in different amplitudes and thus in different mean gray levels. Thus a suitable threshold value cannot be defined in general to binarize the amplitude maps for a fully automatic image analysis. If a uniform threshold value is chosen automatically, many grains are not marked, and some grains are only partially marked. Therefore the nanograins were marked by hand. The area of each marked grain was measured by the particle analysis tool of Gatan Digital Micrograph.

The realization of the binary conversion for a fully automatic image analysis is still in progress. A feasible solution seems to be to binarize each single map before the final add-up. For that purpose, the threshold value has to be adjusted to the intensity values of each single picture automatically.

IV. RESULTS AND DISCUSSION

To record a grain size distribution, the projections of more than 200 nanograins at each sample were measured. From the area projections of the nanograins, the equivalent area diameter was calculated[19] and arithmetically grouped into 14 classes. In Fig. 3, a histogram of the absolute count frequency distribution is shown. The displayed size distributions are numerically fitted by the log-normal function of Eq. (2):

$$P(D) = \frac{A}{(2\pi\sigma^2)^{1/2} D} \exp\left(-\frac{(\ln \mathrm{D} - \ln \mathrm{D}_0)^2}{2\sigma^2}\right) \quad , \quad (2)$$

where D represents the equivalent area diameter of the nanograins, D_o is the median of the distribution, and σ is a shape parameter (i.e., the standard deviation of the Gaussian distribution of log D).

For two observed Gd samples, the calculated GSDs are similar and have essentially the same parameters. This confirms the reproducibility of both the SPS procedure and the analysis method. The GSDs can be well described by a log-normal distribution.

Not all of the nanograins satisfy the Bragg condition. Thus, a fraction of nanograins are not visible in the HRTEM micrographs and not represented in the GSD. It is well known that nanocrystals have a higher tendency to

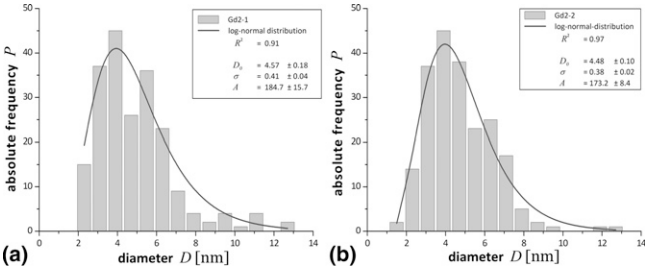

FIG. 3. Grain size distributions in the two Gd samples: (a) Gd2-1 and (b) Gd2-2.

show lattice fringes[20] and to satisfy the Bragg condition from higher misorientations, yielding an increase of the fraction of recorded grains in a given image. The statistical occupancy of the rings in the recorded selected area diffraction pattern (SADP) [Fig. 1(b)] indicates a random orientation of the nanograins that satisfy the Bragg condition. It is most unlikely that the invisible fraction of nanograins shows a crystallographic texture. Thus, we assume a statistical orientation of all the nanograins (no crystallographic texture).

Nanograins that are represented by two sets of lattice fringes allow estimation of the accuracy of grain recognition. A comparison of two different amplitude maps of the same grain revealed in several cases a relative error of less than two percent.

The HRTEM images show only a two-dimensional projection of the grains. Therefore, we have to take into account projection artifacts that cause sampling errors. The sampling errors arise from overlap and truncation effects and generate an underestimation of the fraction of smaller grains.[19] The overlap of nanograins in the foil thickness can be decomposed by the numerical routine (Fig. 4). Usually different grains have a different orientation of their lattice fringes. Thus, they appear in different single pictures, and their overlap can be separated by displaying the concerning single pictures. The effect of truncation is produced by sectioning of nanograins during thinning of the sample. The projection of such a truncation is smaller than the lateral extent of the initial grain. Furthermore, smaller grains have higher probabilities to be removed completely. The fact that the amplitude decreases with decreasing grain thickness[12] reduces the fraction of truncations in a recorded GSD, but it also enhances the underestimation of small grains which is at present unavoidable but considered to be unimportant.

As compared to ADF STEM, the numerical dynamic hollow cone dark-field method presented here has the advantage that the overlap of different nanograins can be disassembled from the single pictures. It is also possible to obtain similar images experimentally by dynamic hollow cone DF TEM. However, due to experimental difficulties, it is hardly possible to apply this method for revealing nano-sized grains. Also, a positioning of the filter mask

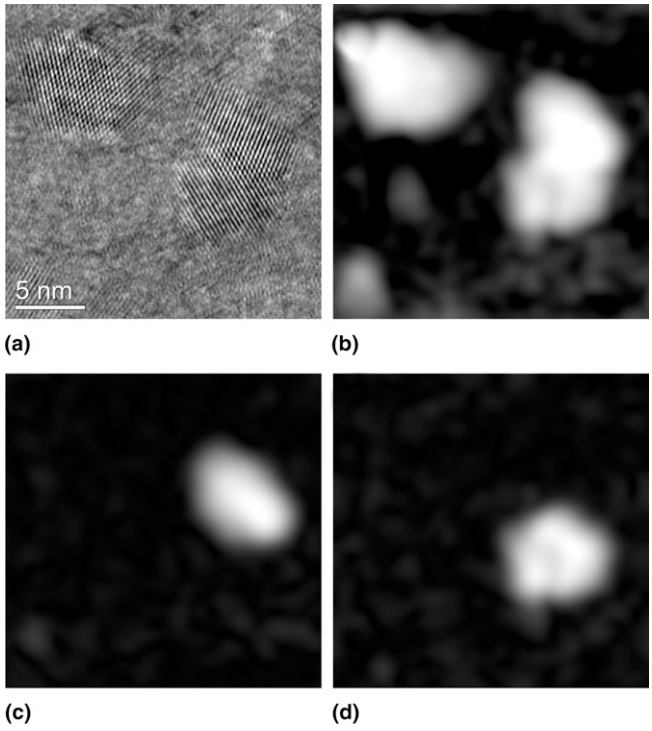

FIG. 4. Disassembling of the overlap of nanograins by the numerical routine: (a) HRTEM micrograph, (b) corresponding amplitude map with overlapping grains on the right side, and (c, d) disassembled grains.

applied to the Fourier spectra numerically is much more precise than the positioning of the object aperture on the diffraction pattern. Compared to hollow cone DF and ADF methods, the numerical filtering method has a higher azimuthal resolution and is more selective.

V. CONCLUSIONS

The presented method generates an amplitude map from a HRTEM picture that contrasts differently oriented nanograins that display the same interplanar spacing. To reduce projection errors, the numerical routine excludes nanograins that exhibit less pronounced lattice fringes. The method is general to all HRTEM images and can also be applied to contrast nanocrystals in an amorphous matrix or to discriminate crystalline nanoparticles to evaluate their size and shape statistically.

The described numerical routine was adapted to determine the GSD in nanocrystalline Gd. The procedure excludes some typical projection errors of TEM, e.g., overlap and truncation effect. In spite of underestimation of smaller nanograins, the recorded GSD follows a log-normal distribution.

In conclusion, the described method is a fast and quantitative way of discriminating nanograins. In addition to the method presented by Hÿtch and Gandais,[10] it is possible to illustrate the contours of different nanograins in one map automatically.

ACKNOWLEDGMENT

The authors are indebted to Robert Bosch Stiftung for financial support.

REFERENCES

1. X.Y. Song, J.X. Zhang, M. Yue, E.D. Li, H. Zeng, N.D. Lu, M.L. Zhou, and T.Y. Zuo: Technique for preparing ultrafine nanocrystalline bulk material of pure rare-earth metals. *Adv. Mater.* **18,** 1210 (2006).
2. E.D. Li, X.Y. Song, J.X. Zhang, and N.D. Lu: Preparation and mechanism study of bulk pure rare-earth metals with amorphous and nanocrystalline structures. *Chin. Sci. Bull.* **52,** 418 (2007).
3. X.Y. Song, J.X. Zhang, E.D. Li, N.D. Lu, and F.X. Yin: Preparation and characterization of rare-earth bulks with controllable nanostructures. *Nanotechnology* **17,** 5584 (2006).
4. M. Yue, J.X. Zhang, H. Zeng, and K.J. Wang: Preparation, microstructure, and magnetic properties of bulk nanocrystalline Gd metal. *Appl. Phys. Lett.* **89,** 32504 (2006).
5. N.D. Lu, X.Y. Song, A.X. Zhang, and E.D. Li: Preparation of Nd bulk with ultrafine nanocrystalline structure and its physical property. *Acta Metall. Sin.* **43,** 739 (2007).
6. R. Mitra, T. Ungar, and J.R. Weertman: Comparison of grain size measurements by x-ray diffraction and transmission electron microscopy methods. *T. Indian Inst. Metals* **58,** 1125 (2005).
7. T. Ungar: Characterization of nanocrystalline materials by x-ray line profile analysis. *J. Mater. Sci.* **42,** 1584 (2007).
8. Z. Liu, D. Shindo, S. Ohnuma, and H. Fujimori: Nano-granular Co–Zr–O magnetic films studied by HRTEM and electron holography. *J. Magn. Magn. Mater.* **262,** 308 (2003).
9. L.S. Karlsson, K. Deppert, and J.O. Malm: Size determination of Au aerosol nanoparticles by off-line TEM/STEM observations. *J. Nanopart. Res.* **8,** 971 (2006).
10. M.J. Hytch and M. Gandais: Quantitative criteria for the detection and characterization of nanocrystals from high-resolution electron-microscopy images. *Philos. Mag. A* **72,** 619 (1995).
11. D.B. Williams and C.B. Carter: *Transmission Electron Microscopy: A Textbook for Materials Science* (Plenum Press, New York, 1996).
12. C. Ricolleau, L. Audinet, M. Gandais, T. Gacoin, and J.P. Boilot: 3D morphology of II-VI semiconductor nanocrystals grown in inverted micelles. *J. Cryst. Growth* **203,** 486 (1999).
13. S. Zghal, M.J. Hytch, J.P. Chevalier, R. Twesten, F. Wu, and P. Bellon: Electron microscopy nanoscale characterization of ball-milled Cu–Ag powders. Part I: Solid solution synthesized by cryo-milling. *Acta Mater.* **50,** 4695 (2002).
14. N. Guigue-Millot, S. Begin-Colin, Y. Champion, M.J. Hytch, G. Le Caer, and P. Perriat: Control of grain size and morphologies of nanograined ferrites by adaptation of the synthesis route: Mechanosynthesis and soft chemistry. *J. Solid State Chem.* **170,** 30 (2003).
15. M.J. Hytch: Analysis of variations in structure from high resolution electron-microscope images by combining real space and Fourier space information. *Microsc. Microanal. M.* **8,** 41 (1997).
16. M.J. Hytch, E. Snoeck, and R. Kilaas: Quantitative measurement of displacement and strain fields from HREM micrographs. *Ultramicroscopy* **74,** 131 (1998).
17. A. Gutakovskii, A. Chuvilin, and S. Song: Application of high-resolution electron microscopy for visualization and quantitative analysis of strain fields in heterostructures. *Bull. Russ. Acad. Sci. Phys.* **71,** 1426 (2007).
18. M.J. Hytch and L. Potez: Geometric phase analysis of high-resolution electron microscopy images of antiphase domains: Example Cu_3Au. *Philos. Mag. A* **76,** 1119 (1997).
19. H.E. Exner: Analysis of grain- and particle-size distrbutions in metallic materials. *Int. Mater. Rev.* **17,** 25 (1972).
20. J.O. Malm and M.A.O. Keefe: Deceptive "lattice spacings" in high-resolution micrographs of metal nanoparticles. *Ultramicroscopy* **68,** 13 (1997).